Proceedings of the 28th IEEE
EMBS Annual International Conference
New York City, USA, Aug 30-Sept 3, 2006

CODED EXCITATION AND ANNULAR ARRAYS FOR HIGH-FREQUENCY ULTRASOUND IMAGING

Jonathan Mamou and Jeffrey A. Ketterling
Frederic L. Lizzi Center for Biomedical Engineering, Riverside Research Institute, New York, NY.

Abstract

High-frequency ultrasound (HFU)shows promises for with fine-resolution imaging. However, the limited depth of field (DOF) and penetration depth of HFU waves mitigates in significance for clinical evaluation. The aim of this study is to use modern annular transducer technology and coded excitation to simultaneously improve DOF and penetration depth. A 20-MHz, five-element annular array with a focal length of 18 mm and a total aperture of 6 mm was custom made using a 25-μm thick polyvinylidene fluoride membrane. The annular array was excited by a 8-μs coded signal to image a phantom made of seven regularly spaced 25-μm wire. The coded signal was a chirp linearly spanning the frequency range 0–40 MHz. Results of this study demonstrate that the DOF can be improved by factor of 3 and and signal-to-noise ratio (SNR) can improved by more than 24 dB with coded-excitation methodologies. The increased SNR offers the potential to increase the penetration depth when imaging in vivo.

1. Introduction

In fundamental ultrasound research and clinical applications, a trend has developed toward operating at higher and higher frequencies over the past two decades. High-frequency-ultrasound (HFU) offers interesting options for noninvasive visualization of living tissues at the microscopic level. HFU imaging is non-ionizing, non-invasive, real-time, and an order of magnitude less expensive than common imaging modalities. HFU image resolution (10-200 μm) cannot be achieved with other clinical imaging modalities such as nuclear imaging, computed tomography or magnetic resonance, which offer resolutions of $\geq$ 1 mm. However, the fine-resolution advantages offered by HFU are offset by limitations in penetration depth that are caused by frequency-dependent attenuation and by limitations in the depth-of-field (DOF) that occur when low F-numbers (the ratio of the focal length to the diameter of the transducer) are employed.

Modern uses of HFU include dermatological evaluation of skin cancer [1], ophthalmic imaging [2], small-animal imaging [3], and *in vivo* imaging via intravascular ultrasound probes [4]. In these applications, tissue assessment is conducted at shallow depths and over a few-millimeter DOF. This study investigates simultaneously improving penetration depth and DOF of HFU. The described approach uses synthetic focusing with annular arrays to increase DOF and modern methodologies using specially designed pulses, termed coded-excitations, to increase penetration depth.

2. Methods

2.1. Annular-array fabrication

The 20-MHz annular array used in these studies was designed and fabricated in house using the techniques described in [5, 6]. The active acoustic layer of the array was a 25-μm thick polyvinylidene fluoride (PVDF) membrane (Ktech Corp., Albuquerque, NM). This membrane was bonded to single-sided, copper-clad polyimide (CCP) film (RFlex 1000L810, Rogers Corp., Chandler, AZ) on which an annular ring circuit pattern had been etched using standard printed circuit board (PCB) techniques. To assemble the transducer, a small quantity of non-conductive epoxy (Hysol RE2039, HD3561, Loctite Corp., Olean, NY) was placed between the film layers and the layers were pressed into a Teflon tube with a stainless steel ball. The assembly was clamped and the Teflon tube was filled with non-conductive epoxy. After the epoxy had cured, the epoxy plug was separated from the Teflon tube and excess PVDF and CCP was trimmed away. The epoxy plug was then mounted into a UHF connector and conductive epoxy (EE129-4 Epoxy Technology, Billerica, MA) provided a ground plane connection between the UHF shell and the PVDF ground electrode.

The final array consisted of five equal-area rings; it had a total aperture of 6 mm and a radius of curvature of 18 mm. The five annuli were separated by 100 μm . Electrical access to the rings was accomplished via trace lines that linked to each annulus on the CCP and necessitated breaking the symmetry of the annuli. However, this had a minimal effect on transducer performance. A PCB was used to link the CCP trace lines to standard BNC cabling. The assembled array was characterized acoustically to validate its operation. Measurements were made in degassed water by placing a quartz plate normal to the transducer axis at the geometric focus. The array had a nominal center frequency of 20-MHz and 6-dB fractional bandwidths near 45% for all elements.

2.2. Data acquisition

The system for exciting and collecting data from the array has been described in detail in [6]. To summarize, the system was designed to automate the process of collecting transmit/receive digital data from all array element combinations. The transducer was scanned across a sample five times, exciting a different ring on each pass. This data was then post-processed for decoding, synthetic focusing, and image generation.

The experimental system consisted of a four-channel dig-

1-4244-0033-3/06/$20.00 ©2006 IEEE.

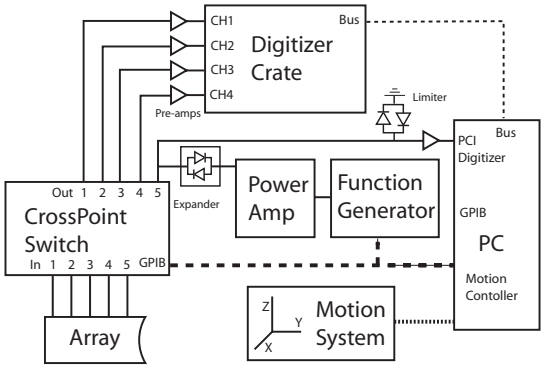

Figure 1: Schematic of experimental system.

itizer crate (DC271 Acqiris, Monroe, NY), a single-channel PCI digitizer (DP110 Acqiris), a bi-directional cross-point switch module (CXL/8X8 Cytec, Penfield, NY), a programmable function generator (33250A Agilent, Palo Alto, CA), a power amplifier (350L ENI, Rochester, NY), and an XYZ motion control system (Fig. 1). Custom, coded-excitation waveforms were downloaded to the function generator and then amplified prior to entering the cross-point switch. The cross-point switch was configured to permit one element of the array to be excited while the remaining four elements were linked to the four-channel digitizer crate. The pulsing channel was routed through a transmit/receive circuit and return echoes were digitized with the PCI based digitizer. Prior to sampling, the crate-digitizer channels were amplified by 45.5 dB in a protected preamplifier (AU-1313 Miteq, Hauppauge, NY) and the PCI digitizer input was amplified by 32.5 dB in a second amplifier (AU-1114 Miteq). Because the electrical path lengths of the two digitizers were different, a relative time delay needed to be added to one of the devices to properly align the signals in time. Because the transmission line had not been fully optimized, the initial data were relatively noisy.

2.3. Synthetic focusing

To improve the DOF and lateral resolution using the annular array, a synthetic-focusing algorithm was employed to post-process the 25 sets of digitized radio-frequency (RF) data [6]. Put simply, focusing at a depth d was achieved by applying the time shifts to and summing the digitized transmit/receive data based on the the equation $t_n = a_n^2(1/R - 1/d)/2c$ [7] where t_n is the one-way delay time for ring n, a is the radius of ring n, and R is the geometric focal distance. The round trip delay time is then found from $t^{tot} = t^{\mathrm{T}} + t^{\mathrm{R}}$ where t^{T} is the transmit delay and t^{R} is the receive delay.

A synthetically focused image is formed by applying the time shift and summing procedure to a series of focal zones, windowing the focal region of each focal zone, and then assembling a final image by splicing all of the focal-zone data together. For a final image with q focal zones, the synthetic-focus process is described by

$$a(t) = \sum_{o=1}^{q} \left(\sum_{l=1}^{n} \sum_{m=1}^{n} E_{l,m}(t - t_l^{\mathrm{T}} - t_m^{\mathrm{R}}) \right) \eta^o(t) \qquad (1)$$

where $\eta^o(t)$ is the rectangular window encompassing only focal zone o and $E_{l,m}$ is the RF data for the transmit/receive ring pair l to m time shifted by $t^{tot} = t_l^{\mathrm{T}} + t_m^{\mathrm{R}}$. If the data are processed with no time delay ($t^{tot} = 0$), the result simulates the case of a single-element transducer.

2.4. Coded excitation

Resolution and penetration are critically important for medical ultrasound imaging. Usually, these two entities present a tradeoff, where one property can be improved only at the expense of the other. However, the use of coded excitation permits this tradeoff to be extended [8] by appropriately coding the transmit signal and decoding the receive signal. Usually the coded signal has a long time duration and the decoding is therefore referred to as compression. Decoding is done by linear filtering of the RF signals by a so-called compression filter.

Theoretically, when the coded signal is a chirp, the SNR gain is equal to the time-bandwidth (TB) product of the chirp [9]. A chirp is a coded signal that linearly spans a frequency bandwidth B where $B = f_2 - f_1$, and f_1 and f_2 are the starting and ending frequencies, respectively. If the chirp sweeps from f_1 to f_2 over a time, T, then the chirp signal is described by

$$s(t) = w(t)\cos\left(2\pi f_1 t + \pi b t^2\right), \qquad (2)$$

where $w(t)$ is a tapering window that vanishes outside of $t \in [0,T]$ and b is the sweep rate equal to $\frac{f_2 - f_1}{T}$. Essentially, the role of $w(t)$ is to mitigate the Fresnel ripple present in the chirp spectrum. Fresnel ripple leads to very strong post-compression range sidelobes which greatly deteriorate image quality [9].

Here, we utilize a 0 to 40 MHz, 8-μs with a 15% Tukey tapering window. In terms of SNR, the best compression filter is typically a matched filter (i.e., the filter whose impulse response is the time-reversed excitation signal). However, using the matched filter for coded excitation imaging leads to large-amplitude range sidelobes that deteriorate the image quality [9]. Therefore, in this study, the compression filter was taken to be the matched filter weighted by a Dolph-Chebyshev window (e.g., mismatched filter) with a prescribed -80-dB sidelobe level. Figure 2 displays the coded excitation signal, the compression filter, and corresponding spectra.

3. Results

To test the methodologies, we utilized a wire phantom consisting of seven 25-μm wires spaced in 1-mm axial and lateral increments. RF data were acquired in three configurations: near, focal, and far. The three configurations corresponded to the nearest wire positioned 9 mm, 15 mm, and

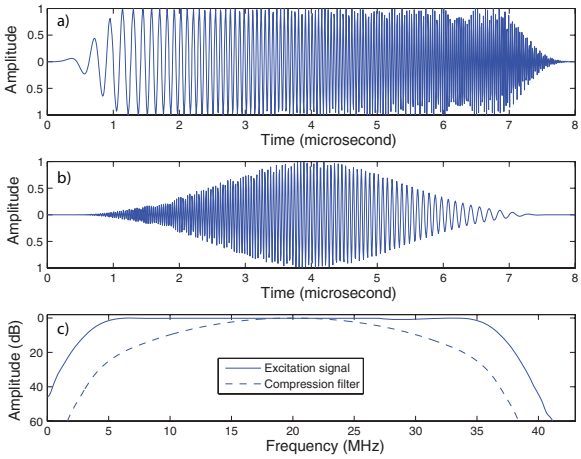

Figure 2: Linear chirp coded excitation signal (a), mismatched compression filter (b), and corresponding spectra (c) used in this study.

21 mm away, respectively, from the transducer surface. Each scan spanned 8-mm and consisted of 321 scan lines spaced 25-μm apart. The RF signals were digitized at 250 MHz and post-processed for compression and synthetic focusing.

To illustrate the long-time duration of the chirp signal, Fig. 3 shows conventional B-mode images obtained in the far configuration with and without synthetic focusing. This figure shows the improved lateral resolution and DOF achieved with synthetic focusing. The images have relatively poor SNRs ($\leq$ 30 dB as displayed in Table 1). The modest SNR is in part due to the electrical transmission line that is not yet fully optimized for coded excitation.

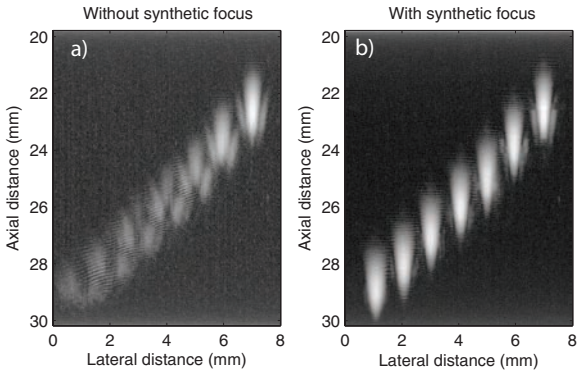

Figure 3: Far images of the wire phantom prior to compression without (a) and with (b) synthetic focusing. The dynamic ranges of the images are 40 dB.

Figure 4 shows the compressed images in all three configurations, with or without synthetic focusing. These images demonstrate three advantageous aspects of our methodologies. First, the axial resolution is restored (i.e., time-signals are brief after compression). Second, the SNR is drastically improved, e.g., by at least 16 dB in the unfocused images and at least 24 dB in the focused images (see Table 1). Finally, the DOF is significantly enhanced in the synthetic-focused images as revealed by the improved resolution of all of the wires, except those nearest to the transducer at the depths 9 and 10 mm [Figs. 4(d-f)].

To quantify the DOF increase, Fig. 5 displays the normalized echo magnitude of each wire for the three configurations with and without synthetic focusing (after compression). It shows that without focusing; only the wires in the range 17–22 mm have a magnitude greater than -10 dB, while with focusing this range increased significantly to 12–28 mm. Based on this simple experiment, it seems that the -10-dB DOF increased by a factor of about 3 from about 5 mm to at least 16 mm.

Finally, Table 1 gathers the SNRs of all twelve images obtained in this study: with and without compression, with and without synthetic focusing, and in the three scanning configurations. The last row of Table 1 displays the SNR improvement after compression. The SNRs displayed in the first row are modest ($<$ 36dB), they show that our system is noisy and optimization of the electronics needs to be pursued actively. The second row shows that compression significantly boosts SNRs for every cases. However, without synthetic focusing, the SNRs remain modest in the near and far configurations. Synthetic focusing allowed us to achieve SNRs above 54 dB, an improvement of at least 24 dB independent of the configuration.

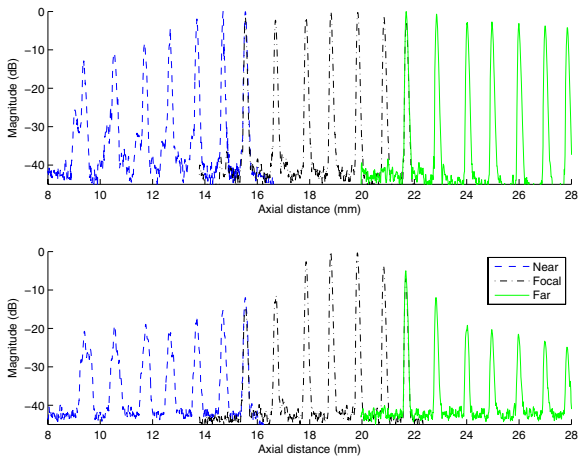

Figure 5: Normalized echo magnitude of each wire after compression with and without synthetic focusing

Table 1: SNR in dB before and after compression.

	Without synth. foc.			With synth. foc.		
	Far	Focal	Near	Far	Focal	Near
Before	29.5	35.8	25.3	30.9	34.4	30.0
After	48.6	54.7	41.9	55.0	57.4	54.3
Impr.	19.1	18.9	16.6	24.1	24.0	24.3

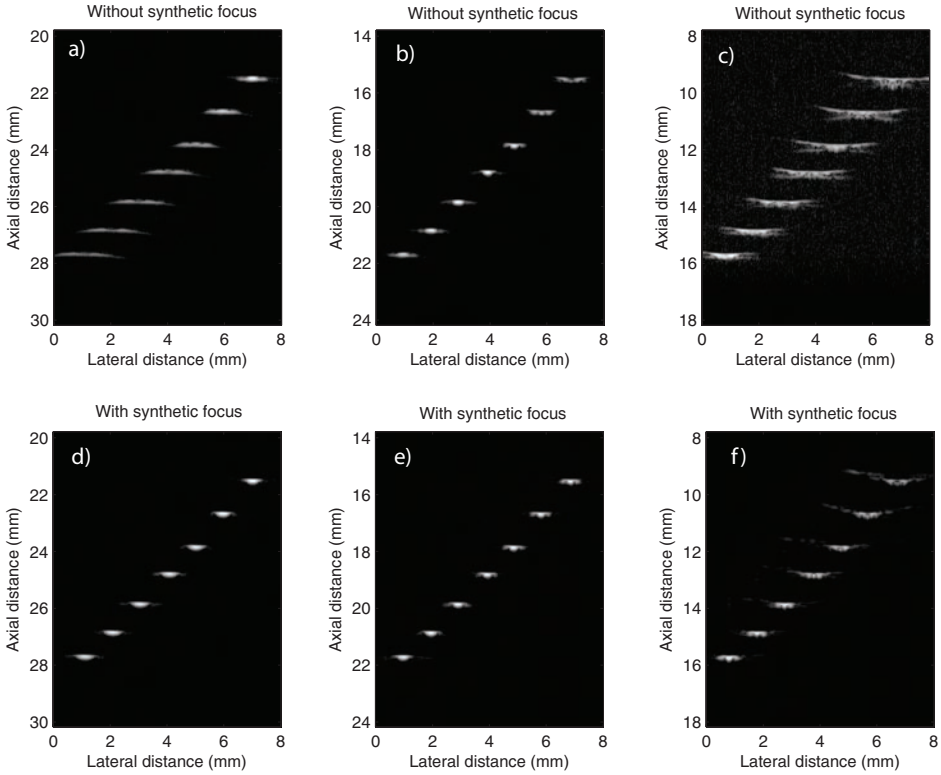

Figure 4: B-mode images of the 7-wire phantom after compression. (a)-(c): Images obtained without synthetic focusing. (d)-(f): Images obtained with synthetic focusing. The dynamic range of the all images is 40 dB and the geometric focus is at 18 mm.

4. Conclusions

This study demonstrates that annular-array technology and coded excitation can improve HFU imaging significantly. The proposed methodologies were able to extend the DOF by a factor of 3 as well as increase the SNR by 24 dB. However, the methodology remains to be evaluated for *in vivo* measurements. Innovative coded excitation and annular arrays methodologies are likely to lead to dramatically improved penetration and DOF for HFU clinical applications.

5. Acknowledgement

This research was supported in part by a grant from the National Institutes of Health (EY014371).

References

[1] M. Vogt and H. Ermert, "Development and evaluation of a high-frequency ultrasound-based system for *in vivo* strain imaging of the skin," *IEEE Trans Ultrason Ferroelectr Freq Control*, vol. 52, pp. 375–385, 2005.

[2] R. H. Silverman, M. J. Rondeau, F. L. Lizzi, and D. J. Coleman, "Three-dimensional high-frequency ultrasonic parameter imaging of anterior segment pathology," *Ophthalmology*, vol. 102, no. 5, pp. 837–843, 1995.

[3] D. H. Turnbull and F. S. Foster, "Ultrasound biomicroscopy in developmental biology," *Trends Biotechnol.*, vol. 20, pp. S29–S33, 2002.

[4] C. L. de Korte, A. F. W. van der Steen, E. I. Céspedes, G. Pasterkamp, S. G. Carlier, F. Mastik, A. H. Schoneveld, P. W. Serruys, and N. Bom, "Characterization of plaque components and vulnerability with intravascular ultrasound elastography," *Phys. Med. Biol.*, vol. 45, no. 6, pp. 1465–1475, 2000.

[5] J. A. Ketterling, O. Aristizábal, D. H. Turnbull, and F. L. Lizzi, "Design and fabrication of a 40-mhz annular array transducer," *IEEE Trans. Ultrason. Ferroelect. Freq. Contr.*, vol. 52, pp. 672–681, 2005.

[6] J. A. Ketterling, S. Ramachandran, and O. Aristizábal, "Operational verification of a 40-mhz annular array transducer," *IEEE Trans. Ultrason. Ferroelect. Freq. Contr.*, vol. 53, pp. 623–630, 2006.

[7] M. Arditi, W. B. Taylor, F. S. Foster, and J. W. Hunt, "An annular array system for high-resolution breast echography," *Ultrason. Imag.*, vol. 4, pp. 1–31, 1982.

[8] R. Y. Chiao and X. Hao, "Coded excitation for diagnostic ultrasound: a system developer's perspective," *IEEE Trans Ultrason Ferroelectr Freq Control*, vol. 52, pp. 160–170, 2005.

[9] T. Misaridis and J. A. Jensen, "Use of modulated excitation signals in medical ultrasound. part II: Design and performance for medical imaging applications," *IEEE Trans Ultrason Ferroelectr Freq Control*, vol. 52, pp. 192–207, 2005.